scientific reports

Check for updates

OPEN

Study on the pore structure evolution and microscopic seepage characteristics of coal under high pressure air blasting

Shaoyang Yan[1,2]✉, Fuqiang Gao[1,2]✉, Xiaolin Yang[3], Huaibao Chu[3], Bo Sun[3,4] & Chang Wang[5]

The pore structure in coal seams has a significant impact on the occurrence and migration characteristics of coalbed methane. The High Pressure Air Blasting (HPAB) is one of the main feasible technologies to improve the efficiency of unconventional gas extraction. Currently, there is little research on the visualization of the evolution of pore structure and seepage characteristics in coal under HPAB, resulting in unclear understanding of the formation of 3D pore network structure in coal under HPAB, the interconnection of pores and fissures, and the mechanism of gas seepage and diffusion under HPAB. Therefore, it is necessary to study the evolution characteristics of pore structure and seepage characteristics of coal under HPAB. The HPAB test was carried out based on a self-developed HPAB device. Statistical analysis of crack propagation law of coal under HPAB from a macroscopic perspective. During the experiment, a microscopic visualization model of coal before and after HPAB was established using CT scanning and Avizo software. The vessel axial skeleton algorithm in Avizo software was adopted to extract the connectivity channels between connected pores and fissures, which realizes the 3D visualization of coalbed methane seepage in the spatial topology structure at the microscopic scale. The seepage, migration, diffusion process and distribution law of coalbed methane in the micro-pore structure of coal have been studied. The mechanism of coalbed methane seepage and migration has been revealed from a microscopic perspective. The research results indicate that: (1) There are four main cracks on the coal surface that approximately run along the direction of principal stress under HPAB and confining pressure. The direction of crack development and propagation in coal under HPAB is influenced by natural defects such as joints and bedding. (2) Before HPAB, the representative elementary volume (REV) of coal has a high degree of curvature in the connectivity channel of pore and fissure. After HPAB, the degree of curvature in the REV is significantly reduced, with a decrease of up to 26.72%. (3) The original micro-pores and newly formed fractures developed and expanded outward under HPAB, forming a relatively developed 3D fracture network channel. Compared with before HPAB, the streamline distribution inside the REV is denser and more numerous. The maximum flow rate and maximum velocity of coalbed methane migration have increased by 112.90 times and 5.24 times, respectively. The research results provide experimental and theoretical basis for improving the efficient extraction of coalbed methane in low-permeability coal seams by HPAB.

Keywords High pressure air blasting, Coal, Evolution of pore structure, Seepage characteristics

In recent years, with the acceleration of urbanization and industrialization in China, the demand for energy has continued to grow rapidly. Shallow resources are gradually depleting, and deep mining has become the new normal for energy development in China[1–3]. With the continuous increase of deep coal mining, the characteristics of coal micro-pores, high ground stress, high gas content, low permeability are increasingly affected by the complex geological conditions in the deep part, which leads to an increase in the difficulty of

[1]School of Intelligent Construction and Civil Engineering, Luoyang Institute of Science and Technology, Luoyang 471023, China. [2]Henan Key Laboratory of Green Building Materials Manufacturing and Intelligent Equipment, Luoyang 471023, China. [3]School of Civil Engineering, Henan Polytechnic University, Jiaozuo 454000, China. [4]School of Civil Engineering, Xinyu University, Xinyu 338000, China. [5]School of Resources and Civil Engineering, Northeastern University, Shenyang 110819, China. ✉email: yanshaoyang1994@126.com; lygaofq@163.com

coalbed methane extraction[4,5]. Therefore, in the process of coalbed methane extraction, improving the fracture development of permeable coal seams and achieving low ecological damage through effective methods is the most worthy scientific issue currently for enhancing the development and utilization rate of coalbed methane resources. The HPAB fracturing technology, as a new type of waterless physical expansion blasting fracturing measure, has outstanding advantages such as environmental protection, energy saving, safety and efficiency, and simple operation. It has been widely applied in the development of unconventional natural gas such as coalbed methane and shale gas[6–8].

The evolution of micro-pore structure (size, distribution direction, connectivity, etc.) in coal rock mass under HPAB affects its macroscopic crack development, propagation, and mechanical properties. Therefore, domestic and foreign scholars have conducted extensive research on the crack propagation and pore structure evolution of coal and rock masses under HPAB using physical experiments, numerical simulations, and on-site testing methods, and have achieved fruitful research results. Some scholars have studied the crack propagation in coal and rock masses under high pressure gas blasting. Wang et al.[9] studied the initiation mechanism, propagation process, and morphology distribution of shale cracks through CO_2 fracturing experiments. Gao et al.[10] conducted high pressure gas blasting tests to test the peak pressure load inside the blasthole and analyzed the influence of different gas pressure conditions on crack propagation. Bai et al.[11] established a model of damage based stress wave propagation-static mechanical equilibrium-gas flow coupling through theoretical analysis to study the crack evolution law in high energy gas fracturing. Zhang et al.[12] established a dynamic model of carbon dioxide blasting rock based on indoor experimental results, which was used to analyze the influence of carbon dioxide blasting on crack propagation and damage effects around the blasthole. The above research found that the development and propagation of cracks in coal rock masses are related to high pressure gas pressure. When the high pressure gas blasting pressure is low, the rock only produces a single crack, and the number of cracks increases with the increase of high pressure gas pressure. Pan et al.[13] used CO_2 pre-cracking blasting to induce cracking in specimens containing voids. The VIC-3D and ultrasonic methods were used to analyze the internal damage and crack propagation laws of coal. It is found that the main crack generated by CO_2 blasting would propagate along the direction of the blasthole, forming a connected main crack between the blasthole and the blasthole. Yang et al.[14] used LS-DYNA software to establish a numerical calculation model of coal under the coupling of HPAB and geostress. It is found that under HPAB, the stress waves inside the coal decay exponentially with increasing distance, and cracks propagate along the direction of maximum principal stress. Chu et al.[15] conducted HPAB simulations of coal using nozzles located 100 mm, 200 mm, and 250 mm away from the orifice to investigate the effect of nozzles on coal fracture. Based on experimental results and fracture mechanics theory, two types of damage fracture models were established for the upper and lower nozzles in the borehole. Zhang et al.[16,17] established a liquid CO_2 phase change pressure model and analyzed the rock breaking mechanism through liquid CO_2 phase change jet experiments. A criterion for determining the phase transition induced cracking of liquid CO_2 in low-permeability coal seams has been proposed. Some scholars have studied the influence of impact loads on the pore structure of coal. Yang et al.[18], Qin et al.[19,20], and Chu et al.[21] used low-temperature liquid nitrogen (LTLN), mercury intrusion porosimetry (MIP), nuclear magnetic resonance (NMR) and other methods to study the changes in pore structure and mechanical properties of coal caused by liquid nitrogen cold impact. It is found that liquid nitrogen cold impact can promote the development of fracture networks and increase the connectivity between micro-pores and macro-pores. Sun et al.[22] studied the changes in coal temperature and pore structure under high-frequency ultrasound by using nuclear magnetic resonance (NMR) and 3D-XRM tomography. It is found that ultrasound can improve the internal temperature of coal and the connectivity between pores and fractures, but its effect on micro-pores and transition pores is not significant. Lin et al.[23] used scanning electron microscopy (SEM), energy dispersive spectroscopy(EDS), and mercury intrusion porosimetry (MIP) to study the pore structure changes of smokeless coal treated with different concentrations of NaCl solution under high-voltage electric pulses. Zhang et al.[24] characterized the micro-pore structure changes of coal and raw coal before and after dynamic impact with a pendulum using an ultrasonic tester. Yan et al.[25] and Liao et al.[26] used scanning electron microscopy (SEM), mercury intrusion porosimetry, and CT scanning methods to study the pore structure characteristics of coal at different positions from the blasthole. Wang et al.[27] and Li et al.[28] simulated stress wave impact on coal samples using SHPB. The pore structure of coal samples before and after SHPB impact was characterized using mercury intrusion porosimetry (MIP) and low-temperature liquid nitrogen (LTLN). Li et al.[29] and Li et al.[30,31] characterized the pore structure of different shale facies using experimental methods such as X-ray diffraction (XRD), scanning electron microscope (SEM), mercury intrusion porosimetry (MIP), and low-temperature liquid nitrogen (LTLN). Xia et al.[32] and Bai et al.[33] combined mechanical experiments, scanning electron microscopy (SEM), and mercury intrusion porosimetry (MIP) to study the effect of stress waves generated by liquid CO_2 phase change fracturing (LCPCF) on the pore/fracture structure of coal. The above research found that stress waves and high press gas blasting can cause irreversible damage to the micro-pore structure of coal, and can induce the evolution from isolated closed pores to open pores, improving the connectivity of the coal. At present, researchers have quantitatively and qualitatively characterized the evolution of pore structure and distribution characteristics of pores and fissures in coal rock masses before and after dynamic load impact using low-temperature liquid nitrogen (LTLN), mercury intrusion porosimetry (MIP), nuclear magnetic resonance(NMR), and scanning electron microscopy (SEM). However, the research on the characterization of the 3D pore structure in coal under HPAB is not yet complete. Especially, In terms of the formation of the 3D pore network structure and the mechanism of coalbed methane seepage and diffusion in coal under HPAB.Therefore, it is urgent to conduct in-depth research on the evolution of 3D pore structure and coalbed methane diffusion process in coal under HPAB.

In this paper, the crack propagation law of coal under HPAB is studied by using a self-developed HPAB device from a macro perspective.the microscopic scale visualization models of coal before and after HPAB were established using CT scanning and Avizo software. The 3D visualization of coalbed methane flow in the

Fig. 1. The schematic diagram of coal.

Number	Industrial analysis/%				$R_{o,max}$/%	Microscopic organic components/%		
	Ash (A_d)	Moisture(M_{ad})	Volatile(V_{daf})	Fixed carbon(FC_{ad})		Vitrinite group	Inertinite group	Shell group
1	7.83	2.43	5.92	83.82	2.97	84.9	8.9	/
2	7.53	2.61	6.53	83.33	2.47	88.7	2.8	/
3	8.12	2.32	6.12	83.44	3.10	77.7	4.2	/

Table 1. Summary of industrial analysis and test results of coal samples.

Mix proportion	Cement	Sand	Gypsum	Water	Perlite	Mica	Foaming agent
	100	280	14	43	2	2	0.35
Average value of simulated coal test results	Compressive strength/MPa	Tensile strength/MPa	Density/kg/m^3	Poisson's ratio	Wave velocity/m/s	Porosity	Elastic modulus/GPa
	12.82	1.06	1.638	0.26	2152	6.68	2.52

Table 2. The mix proportions and test results of simulated coal (kg/m^3).

spatial topological structure at the microscale is achieved using AVIZO software. The formation mechanism and distribution characteristics of seepage channels in the REVs before and after HPAB are analyzed. The migration and diffusion process and distribution law of gas in the microscopic porous medium structure were explored from a micro perspective.

Methodology

Experimental study on failure morphology of coal under HPAB

Specimens preparation

The experimental object is smokeless coal from the 11,060 working face of Zhaogu Coal Mine in Jiaozuo Coal Group. The coal seam in the 11,060 working face of Zhaogu Mine belongs to the Shanxi Formation of the Lower Permian, mainly composed of block coal with a small amount of granular coal interbedded. The internal fractures are developed, and the strength of the block coal is high. The macroscopic coal rock composition is mainly composed of bright coal, followed by dark coal, and contains a small amount of filamentous carbon lenses. Considering the strong heterogeneity of coal, smokeless coal with dimensions not less than 200 mm is selected as the object. The schematic diagram of coal is shown in Fig. 1.The average strength coefficient and apparent density of the tested coal block are 1.32 and 1.52 g/cm^3, respectively. The summary of industrial analysis and testing of selected coal is shown in Table 1.

Due to the poor flatness of the coal block shape, it is not conducive to constrained loading during the experiment. In order to better study the fracture characteristics of the coal and the permeability and migration characteristics of coalbed methane under confining pressure and HPAB. The simulated materials were selected to fully wrap the coal to make model specimens. The physical and mechanical basic parameters of specimens made of simulated materials have a high degree of fit with the coal. The mix proportions and test results of simulated coal are shown in Table 2. It should be noted that the model test specimens is made using a mold with a size of 500 × 500 × 500 mm. The production process of the model specimen is shown in Fig. 2.

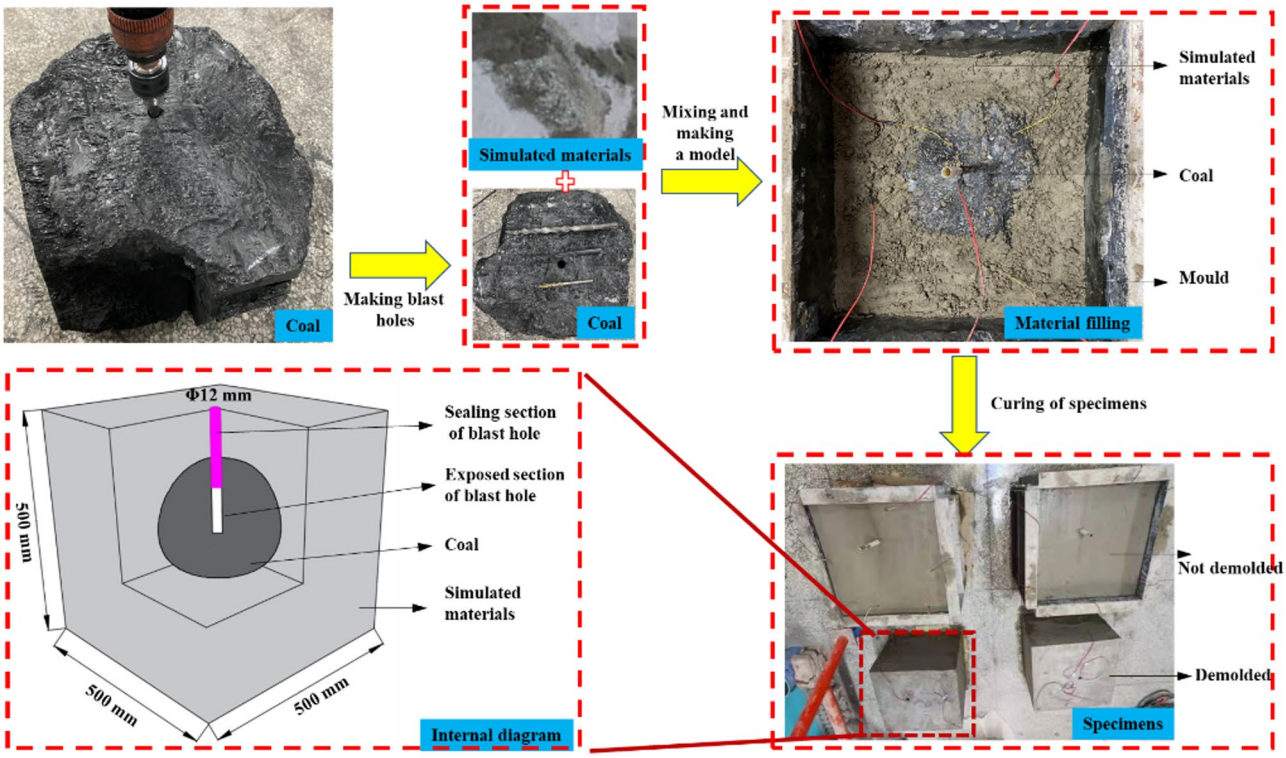

Fig. 2. The production process of the model specimen.

High pressure air blasting (HPAB) test

The self-developed HPAB test device is used to conduct HPAB tests. The HPAB device mainly consists of three parts[34]: (1) gas pressurization and control release system, (2) bidirectional pressurization system, (3) data acquisition system. The high-pressure air blasting (HPAB) device is shown in Fig. 3. In the HPAB test, in-site stress $\sigma_1 = \sigma_2 = 4$ MPa, the air pressure was set over 15 MPa, are applied to the specimens. Due to the randomness and uncertainty of HPAB tests, a total of 4 model specimens were made to ensure the smooth completion of the tests. During the experiment, a vertically downward blasthole with a depth of 300 mm and a diameter of 12 mm is reserved in the middle of the specimen. The fracturing pipe as fixed at a height 50 mm away from the bottom of the blasthole by planting adhesive. The surface around the specimen is coated with a layer of the coupling agent with a thickness of 4–6 mm to avoid the error caused by boundary effects. During the loading process, it should be ensured that the pressure plate contacts the boundary surface of the test block.

Microscopic seepage characteristics of coal under HPAB

Sampling of the specimens and industrial CT

The acquisition of specimens is the key technology to studying the characterization of microscopic pore structure before and after HPAB. Therefore, the samples size of $10 \times 10 \times 30$ mm at a distance of 50 mm from the blasthole were obtained by a cutting machine with strong anti-interference ability. The samples was subjected to CT scanning using an industrial CT produced by Phoenix company. The specific parameters of the test conditions are as follows: the current is 110 μA, the voltage is 150 kV, the minimum spatial resolution is 5 μm, the pixel is 2024×2024, and the number of slices is 1000. The industrial CT scanning flow chart is shown in Fig. 4.

3D pore network model and topological skeleton structure model

In the process of CT scanning, electronic devices and X-ray sources have interference effects on the sample scanning results, such as stains and noise, so it is impossible to conduct vector operation on the scanned image directly. Therefore, the image processing software should be used to remove the interference information of the scanned image. As is well known, three filtering algorithms, Gaussian filter, Mean filter, and Median filter, are applied to image processing. Comparing the performance of the three algorithms, it was found that the median filtering denoising method had better results. The median filtering method is used for denoising CT slices. Given that the skeletal structure and pore information on CT slices are divided by pixel points.The information in CT slices is accurately and effectively extracted by adjusting the size of grayscale feature values, providing a foundation for accurately establishing 3D models.

The noise processing of CT slices and the establishment of 3D visualization models can be achieved using AVIZO software. Considering the storage and model computation time of the computer, after repeated debugging, a cube with dimensions of $1.85 \times 1.85 \times 1.85$ mm was selected as the REV to establish a 3D visualization model. In order to reveal the connectivity characteristics of the geometric spatial structure of pores before and after HPAB. Based on a 3D pore model, a reasonable distance transformation is performed on the 3D topological

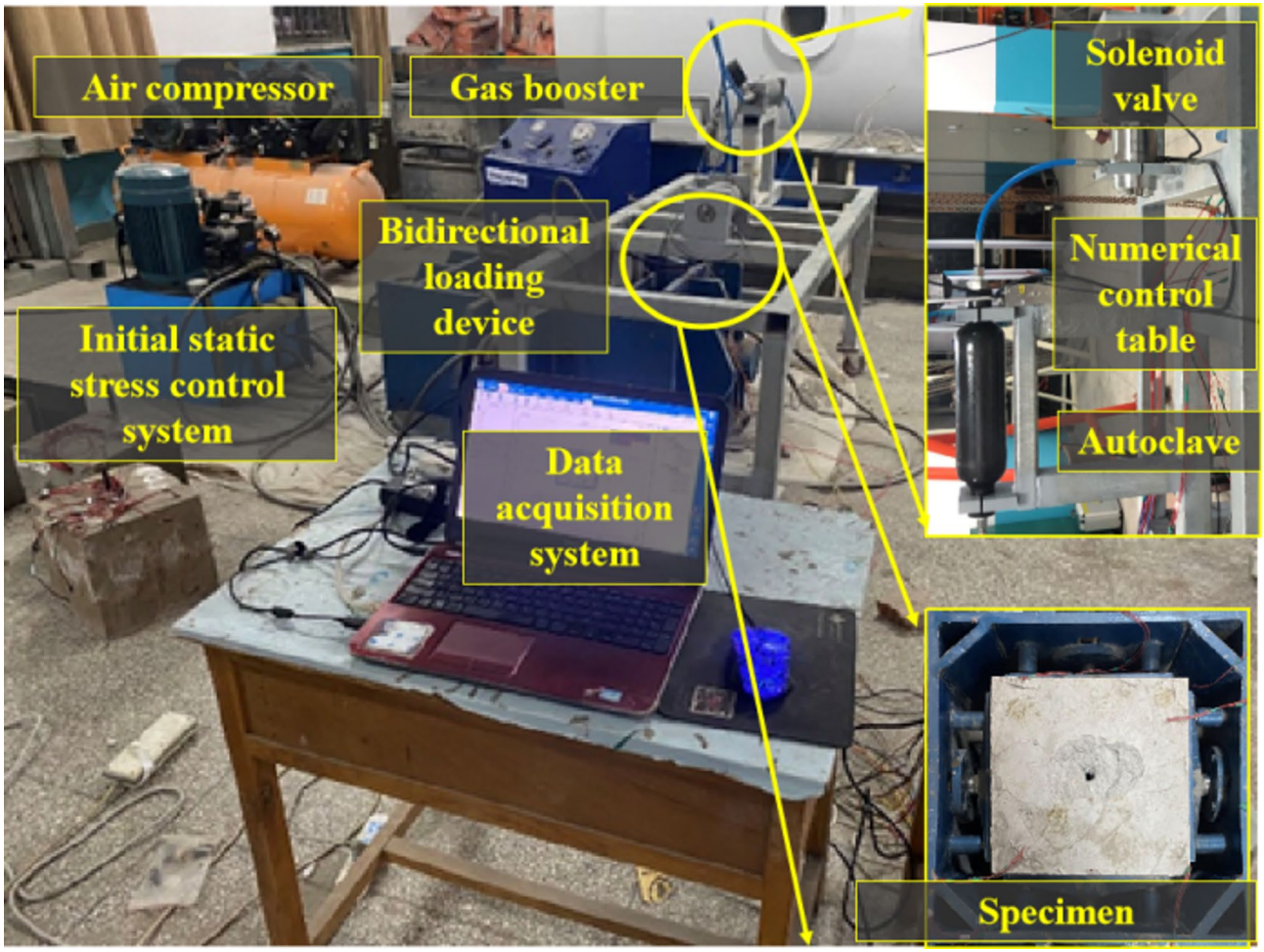

Fig. 3. The high-pressure air blasting (HPAB) device.

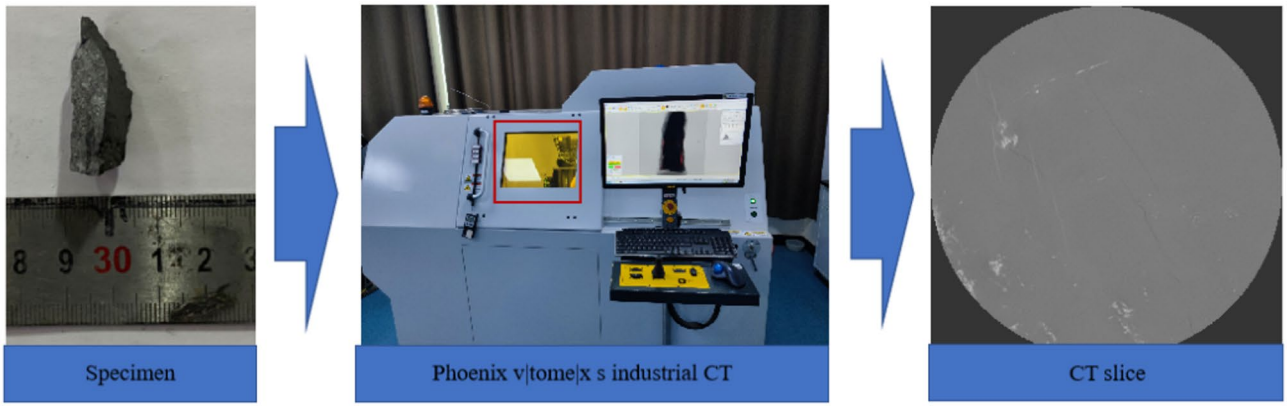

Fig. 4. Industrial CT scanning flow chart.

spatial form of the pore fissure using the vessel axial skeleton algorithm. Simplify the pore fracture structure in the RVE into a 3D topological skeleton structure model. The CT slice preprocessing and 3D visualization process are shown in Fig. 5.

Seepage simulation control equations and boundary conditions

(1) Model processing.

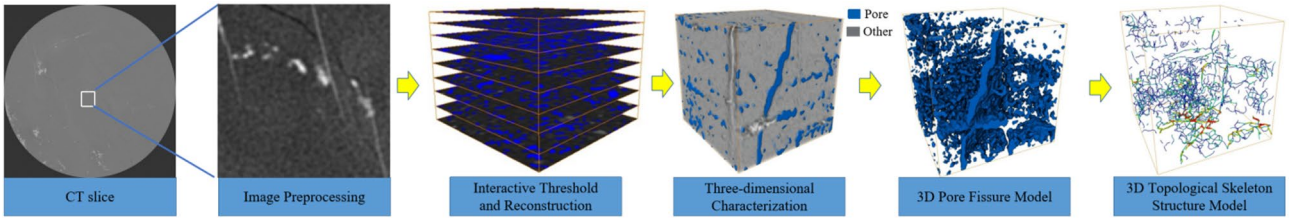

Fig. 5. CT image preprocessing and 3D visualization process (the image was created using AVIZO 2019.1 and PowerPoint 2016).

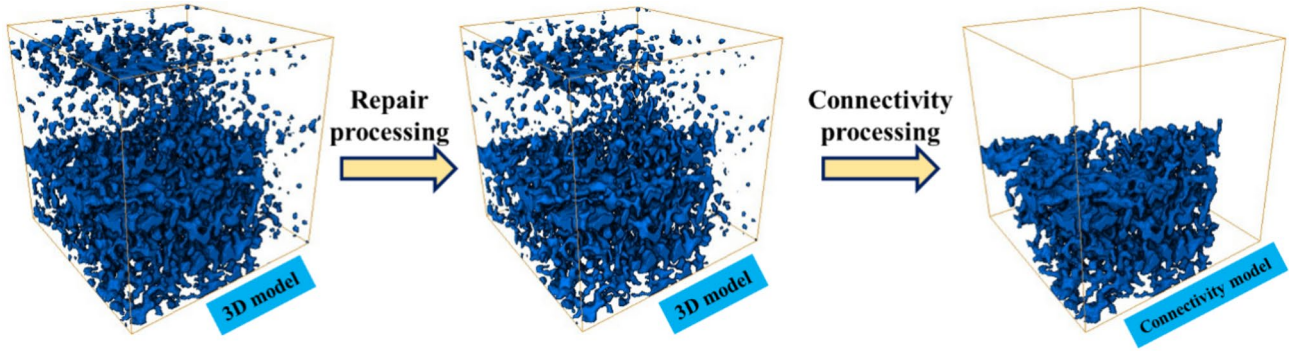

Fig. 6. Extraction and processing of connectivity model.

Before conducting microscopic flow simulations on the REV. Firstly, the pores and fissures in REV were repaired using the embeded repair of AVIZO software. Then, the connectivity model of pore and fissures is extracted using connectivity algorithm. Finally, the details of the connectivity model are repaired and processed using the embeded repair of AVIZO software. The extraction and processing process of the connectivity model of pores and fissures is shown in Fig. 6.

(2) Control equation.

The Xlab module in Avizo software is used to implement visual seepage simulation in the pore and fissure structure. Assuming that coalbed methane is transported as an incompressible gas under standard (normal temperature and pressure) conditions during the simulation experiment. The Navier-Stokes (N-S) equations are used as the governing equations for visual seepage simulation of coalbed methane .The N-S equation form acting on a small volume unit can be expressed as:

$$\rho\frac{dv}{dt} = -\nabla p + \mu\nabla^2 v + \frac{1}{3}\mu\nabla(\nabla\cdot v) + \rho f \tag{1}$$

According to the continuity equation, the mass of coalbed methane flowing in and out of a small volume unit is equal. The mass conservation equation inside the volume unit can be obtained as follows:

$$\frac{\partial\rho}{\partial t} + \nabla\cdot(\rho v) = 0 \tag{2}$$

Given that coalbed methane is incompressible and its density remains constant during flow and transport, Eq. (2) can be transformed into:

$$\frac{\partial\rho}{\partial t} = \nabla\cdot(\rho v) = \nabla\cdot v = 0 \tag{3}$$

Based on the above assumptions, the incompressible equation within a finite volume element can be simplified as:

$$\begin{cases}\nabla\cdot v = 0\\ \mu\nabla^2 v - \nabla p = 0\end{cases} \tag{4}$$

Flow state of coalbed methane	Density(ρ)	Dynamic viscosity(μ)	Inlet pressure(P_{in})	Outlet pressure(P_{out})
Steady-state flow	0.714 kg/m^3	1.85×10^{-5} Pa·s	1.1 MPa	0.1 MPa

Table 3. Specific relevant parameters of seepage visualization simulation.

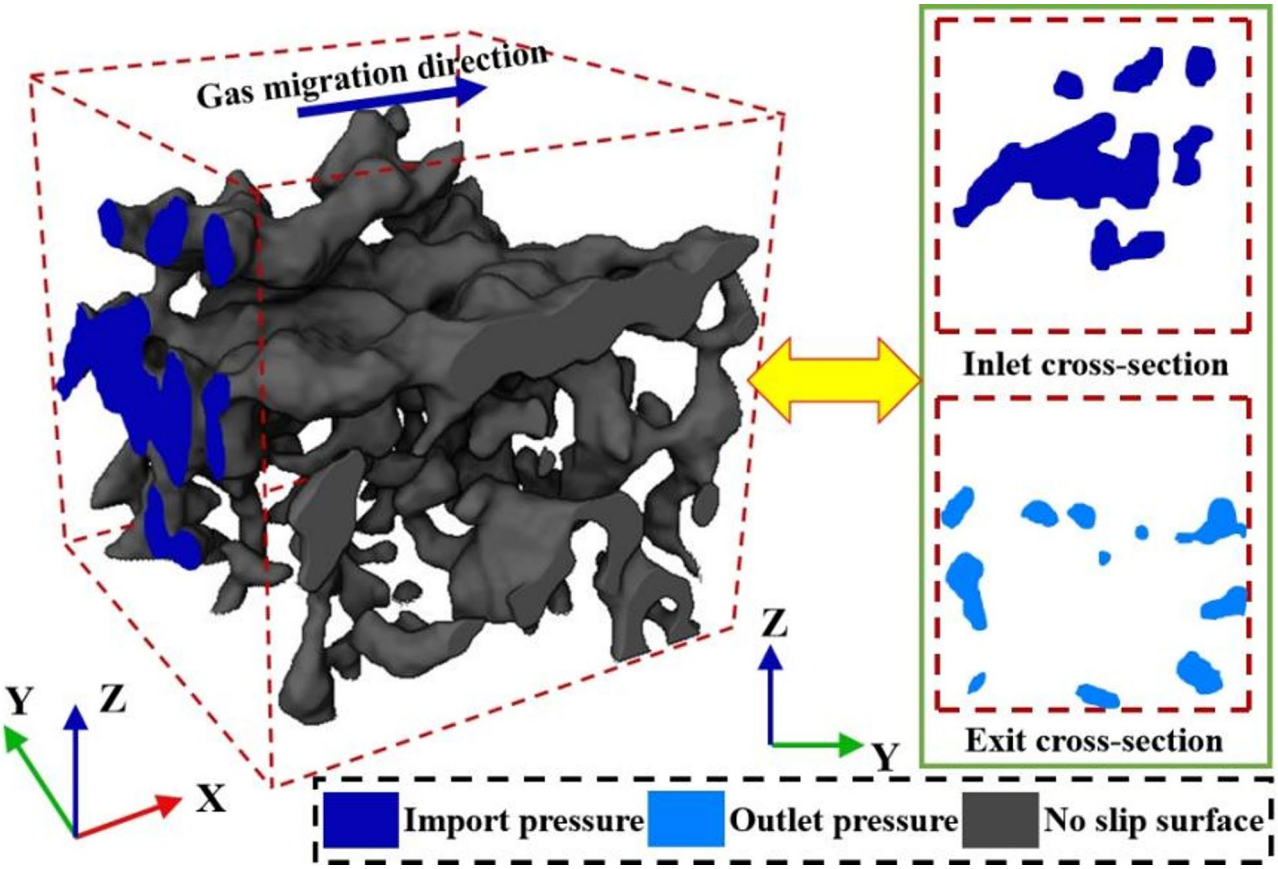

Fig. 7. Schematic diagram for boundary setting of seepage visualization geometric model (the image was created using Avizo 2019.1 and PowerPoint 2016).

In the formula:$\nabla$is the gradient operator; ν is the flow rate of coalbed methane, m/s; μ is the dynamic viscosity of coalbed methane, Pa·s; ∇^2 is the laplacian operator; p is pressure of coalbed methane, MPa; $\rho$is thedensity of coalbed methane, kg/m^3.

(3) Boundary conditions and simulation parameter settings.

The boundary conditions are set as follows:① The interface between fluid and solid is a slip free surface. ② The closed system isolated from the outside world. ③ The fluid pressure is quasi-static and the fluid can freely diffuse on the input surface. ④ The fluid is incompressible and in a steady-state flow state.

Simulation parameter setting: ① The coalbed methane under normal temperature conditions is a simulated fluid medium. ② The two opposing sides are the inlet and outlet for gas flow. The specific relevant parameters are shown in Table 3.Considering that high-pressure air blasting has a significant impact on the microstructure of coal. Visual simulation is conducted from three different directions: X, Y, and Z. Taking the simulation in the X direction as an example, the boundary conditions are set. The specific boundary condition setting diagram using AVIZO and PowerPoint is shown in Fig. 7.

Results and discussion

Analysis of the failure morphology in coal under HPAB

Analysis of the distribution characteristics in coal under HPAB

The failure Morphology of coal under HPAB is shown in Fig. 8.

As can be seen in Fig. 8, under the current test conditions, there is no fracture zone around the blasthole. There are four main cracks on the coal surface that approximately run along the direction of principal stress under HPAB and confining pressure.The direction of crack development and propagation in coal under HPAB

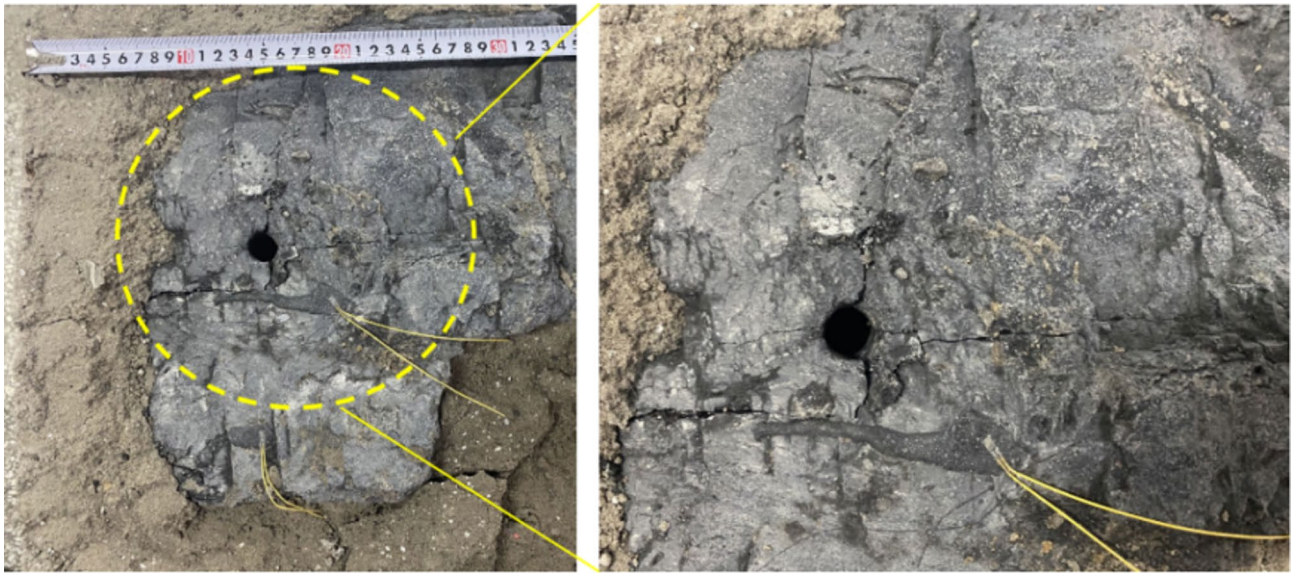

Fig. 8. Failure morphology of coal under HPAB.

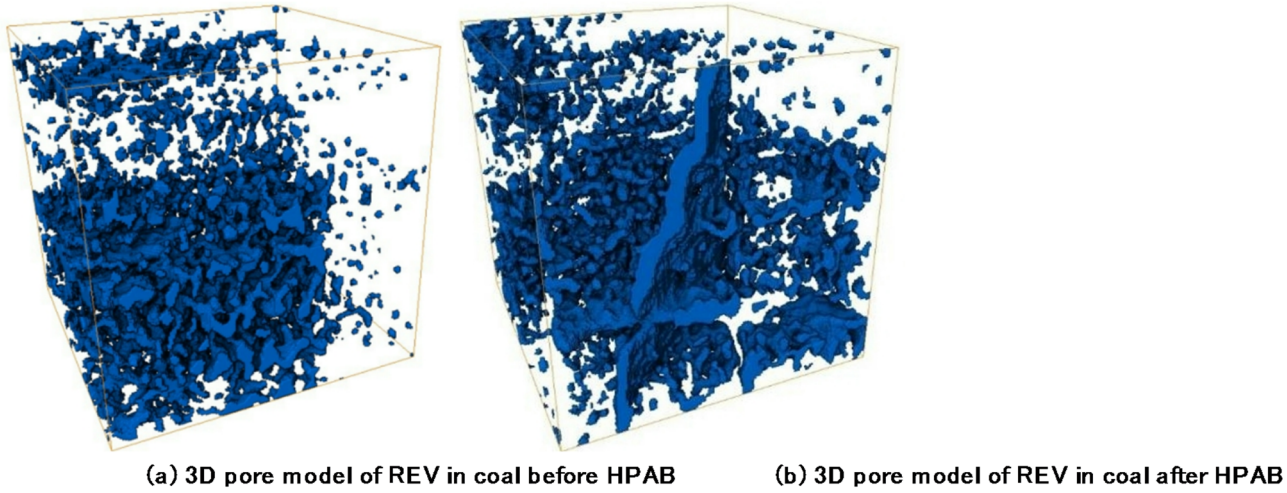

Fig. 9. 3D pore model of REV in coal before and after HPAB (The image was created using AVIZO 2019.1).

is influenced by natural defects such as joints and bedding. The crack propagation around the blasthole is mainly caused by stress waves. The stress waves decay rapidly with the increase of distance from blasthole, and the crack propagation in the middle and far area of the explosion source is mainly caused by stress waves and high-pressure air infiltration and disturbance. Under HPAB and confining pressur, randomly distributed micro-cracks develop and propagate along the direction of maximum confining pressure to form main cracks, while cracks that propagate in other directions are suppressed.

Distribution characteristics of coal pore and fissure channels under HPAB

The 3D pore model and the 3D topological skeleton structure model of the REV in coal before and after HPAB using AVIZO software are shown in Figs. 9 and 10, respectively.

The conclusions drawn from Figs. 9 and 10 are as follows: The changes in pore size and connectivity of coal under HPAB can can be determined by the colors of channels and nodes between channels in the 3D topological skeleton structure model. the colors of channels and nodes between channels in the 3D topological skeleton structure model of the REV. Among them, the transition of channels and nodes in RVE from light blue to red indicates the evolution of pore and fissure size and the connected channels between pores and fissures from few to many. In the 3D topological skeleton model of the REV in coal before HPAB, the number of red areas is relatively small, while the number of light blue areas is relatively large, indicating poor connectivity of coal before HPAB. Compared with before HPAB, there are more red colored areas in the 3D topological skeleton model of REV in coal after HPAB. The pores and fissures in coal develop from randomly distributed isolated closed

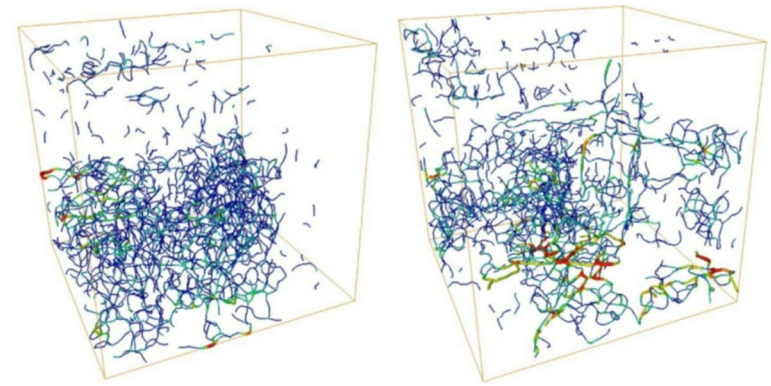

(a) 3D topological skeleton structure model of REV in coal before HPAB

(b) 3D topological skeleton structure model of REV in coal after HPAB

Fig. 10. 3D topological skeleton structure model of the REV in coal before and after HPAB (the image was created using AVIZO 2019.1).

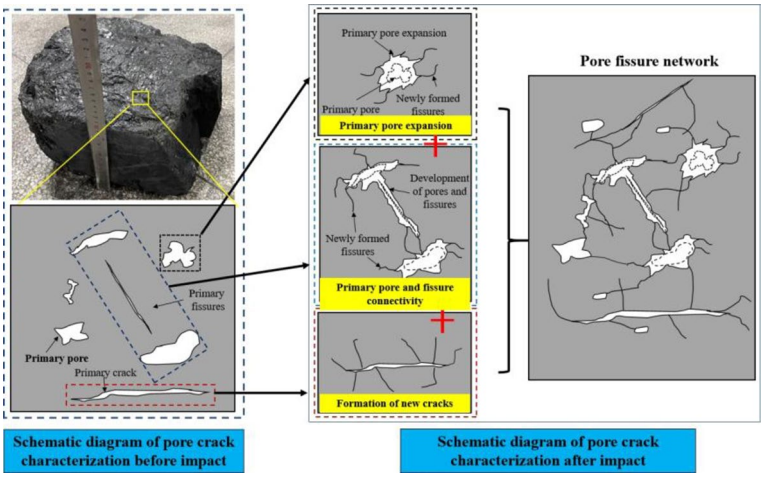

Fig. 11. The schematic diagram of the development of pores and fissures in coal under HPAB.

pores to concentrated connected fractures under HPAB. During HPAB process, the size of pore and fissure and number of connected points in the 3D topological skeleton structure model of the REV have increased, resulting in an increase in the number of red colored areas.

Analysis of the mechanism of pore and fissure development in coal under HPAB

Considering that coal contains randomly distributed and differently shaped initial damages (such as micro-pores, micro-cracks, bedding). Based on the development of pores and fissures at the micro-scale and fracture characteristics at the macro-scale. The evolution and expansion model of pore and fissure development in coal under HPAB is analyzed. The development of pore and fissure structures in coal under HPAB mainly includes the expansion and development of existing pores and fissures, the expansion and penetration of existing pores and fissures, and the initiation and development of new fissures. The schematic diagram of the development of pores and fissures in coal under HPAB is shown in Fig. 11.

As can be seen from Fig. 11, before HPAB, the coal contains primary pores and fissures of various shapes that are not connected to each other.The development and expansion of pores and fissures in coal form a complex 3D network structure under HPAB. The stress waves generated by HPAB can induce the movement of mineral particles around the primary pores in coal, leading to a decrease in the bonding between particles and promoting the expansion and outward development of primary pores and fissures. At the same time, it will be accompanied by the emergence and development of new fissures. The volume of primary pore fissures and the number of

newly formed fissures in coal are increased under HPAB, which promotes the connection and connection between newly formed fissures and primary pores and fissures.

The stress wave generated by HPAB can cause tensile stress to appear around the pores and fissures with different shapes and random distributions in coal, which leads to the development and expansion of the pores and fissures along the position with the minimum stress concentration during the development process. The orientation of the minimum point of stress concentration in coal of pores and fissures is greatly influenced by their morphology and distribution. Therefore, the interdependence between coal pores and fissures during their development and expansion is enhanced under HPAB, which increases the complexity of the 3D network structure between primary pores and fissures and newly formed fissures.

Simulation and analysis of 3D visualization seepage characteristics of coal under HPAB

The permeability is an important parameter used to characterize the permeability of coal, while seepage pressure and velocity are also important factors in measuring the effectiveness of gas migration and flow[35,36]. During the migration of coalbed methane in different directions, different seepage characteristics are affected by the anisotropy of the coal. Therefore, the Avizo software embedded algorithm is used to extract connectivity models and 3D topology skeleton model of coal before and after HPAB, as shown in the Fig. 12.

The absolute permeability, migration pressure, and migration velocity of coalbed methane in different directions of the REV connectivity model are characterized. The seepage patterns in different directions in the connected model of the REV before and after HPAB were explored. The seepage and migration results of coalbed methane in the connectivity model of REV before and after HPAB is shown in Table 4.

Distribution of gas migration pressure field in REV before and after HPAB

The distribution of gas migration pressure fields in different directions in REV before and after HPAB using AVIZO software are shown in Fig. 13. The relationship between gas migration direction and tortuosity in REV before and after HPAB is shown in Fig. 14. The color change between connected pores and fissures in RVE is used to characterize the pressure changes of gas migration.

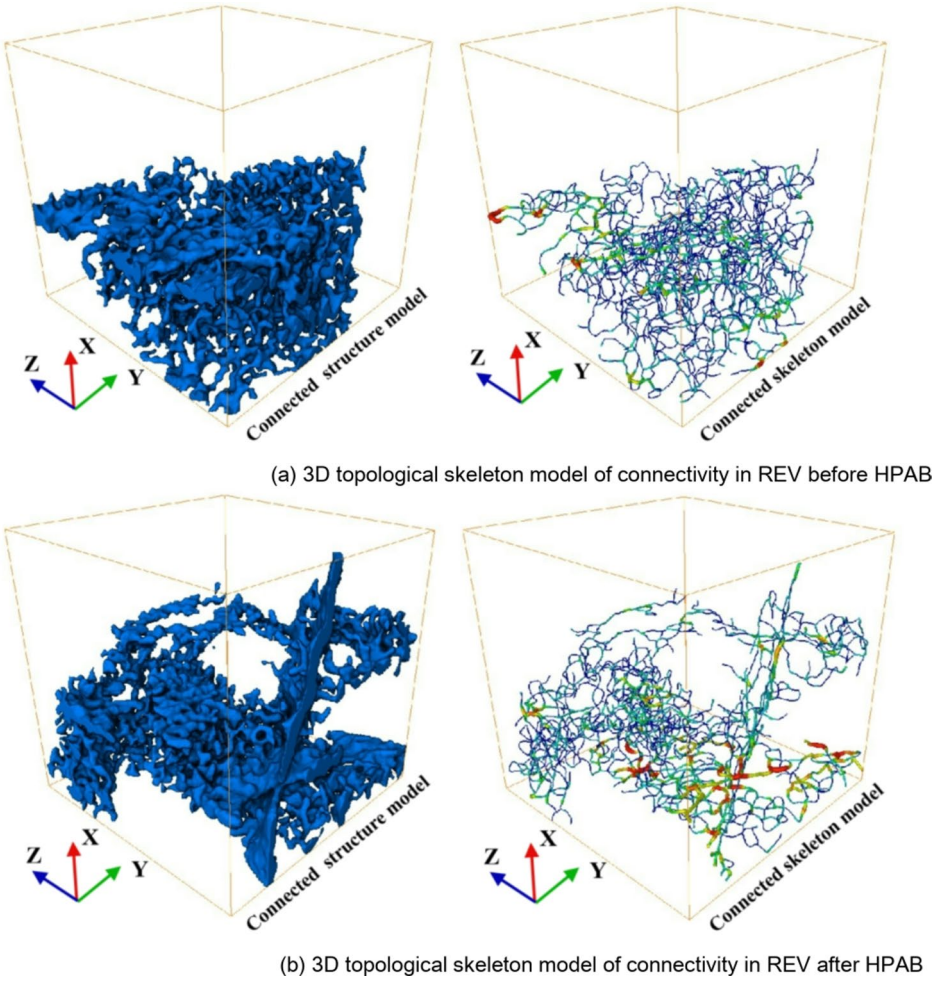

Fig. 12. 3D topological skeleton model of connectivity in REV before and after HPAB.

Parameter	Gas migration direction before HPAB			Gas migration direction after HPAB		
	X	Y	Z	X	Y	Z
Model size	1.85 × 1.85 × 1.85 mm					
Absolute permeability μm^2	0.022	0.129	0.015	0.076	1.078	1.560
The average value of absolute permeability	0.055			0.905		
Tortuosity	2.104	1.763	1.774	2.057	1.518	1.292
Maximum flow($\times 10^{12}$)μm^3/s	1.368	7.784	2.293	7.420	105.642	154.447
Maximum flow rate($\times 10^{9}$)μm/s	1.845	3.144	2.772	4.114	10.770	16.465

Table 4. The permeability and migration results of coalbed methane in the connectivity model of REV before and after HPAB.

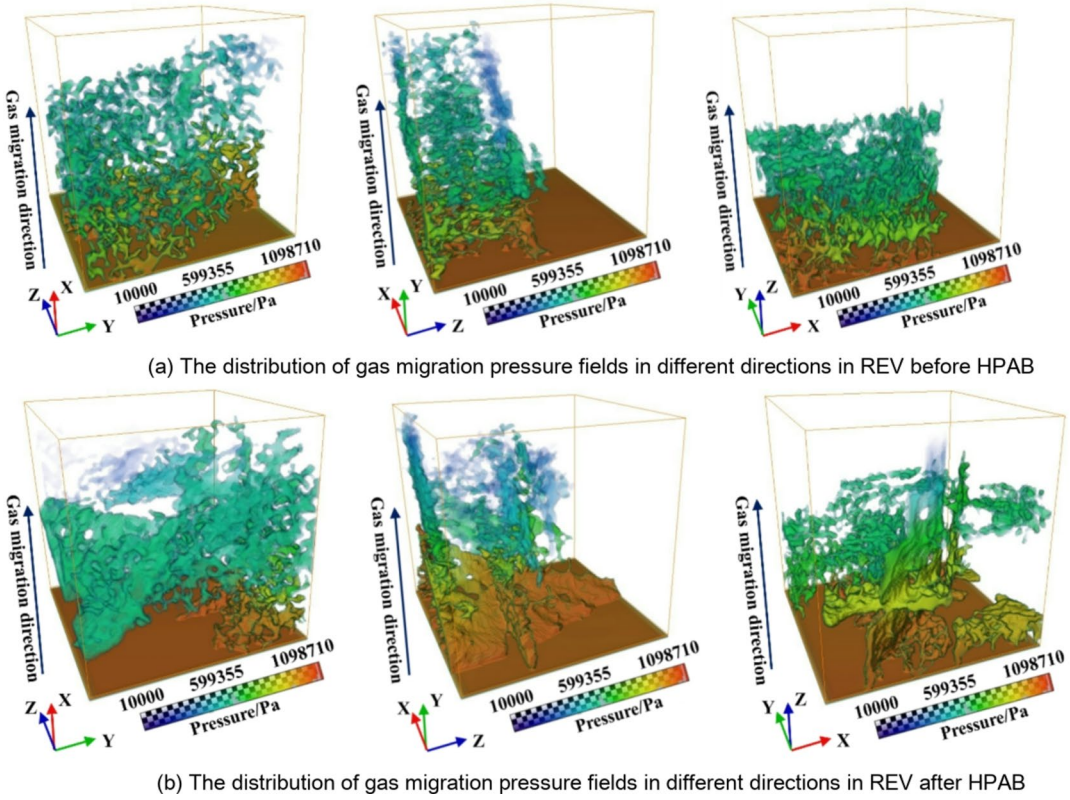

Fig. 13. The distribution of gas migration pressure fields in different directions in REV before and after HPAB (The image was created using AVIZO 2019.1).

The conclusions drawn from Figs. 13 and 14; Table 4 are as follows: Under the condition of the same pressure difference in gas migration between the inlet and outlet of REV, the gas migration pressure shows a decreasing trend during the migration process along the pores and fissures connected channel, that is, the red color at the inlet gradually evolves towards the blue color at the outlet. The parameters such as the range of connected pores and fissures, the radius and length of connected pores and fissures, and the tortuosity of connected channels in the REV of coal before HPAB are mainly determined by the anisotropy of coal, which leads to significant differences in the pressure distribution range during gas migration. In the X direction, the pressure distribution range of gas migration in REV is relatively dispersed, with a tortuosity of 2.104. The gas pressure in RVE drops sharply, with a relatively high proportion in the range of 0.5–0.9 MPa. Compared with the X direction, the curvature of the Y and Z directions in REV is lower, with a tortuosity of 1.763 and 1.774, respectively. The gas migration pressure in RVE is relatively high within the range of 0.7 ~ 0.8 MPa.

The development and expansion of pores and fissures in coal are caused by stress waves generated by HPAB. The randomly distributed pores and fissures in the coal develop along weak points under the action of stress waves. The number and size of connecting channels between coal pores and fissures of REV in coal are increased. The tortuosity of connecting channels between pores and fissures of RVE in coal is reduced. The tortuosity of RVE in the X, Y and Z directions after HPAB is 2.057, 1.518 and 1.292, respectively. Compared with before

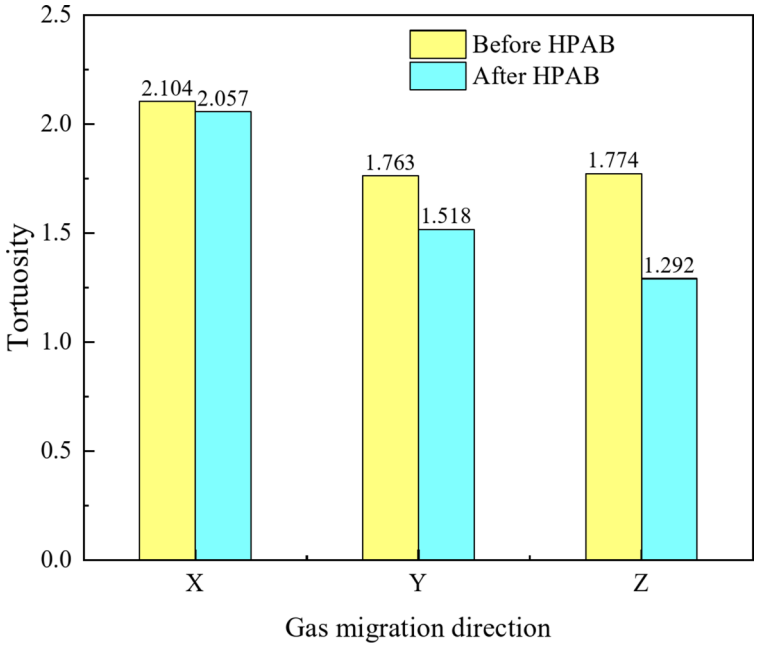

Fig. 14. The relationship between gas migration direction and tortuosity in REV before and after HPAB.

HPAB, the tortuosity in the RVE Z and Y directions is significantly reduced after HPAB, the tortuosity have reduced by 27.17% and 13.90%, respectively. The pressure of gas migration shows a steady-state decreasing trend, with gas migration pressure mostly concentrated in the range of 1.0 ~ 1.05 MPa.

Distribution of gas migration velocity field in REV before and after HPAB

The distribution of velocity fields in the X、Y、Z directions of gas migration in REV before and after HPAB using AVIZO software are shown in Fig. 15. The relationship between gas migration direction and maximum flow rate in REV before and after HPAB is shown in Fig. 16. The migration characteristics of gas between connected pores and fissures in REV can be characterized by parameters such as the color, size, and density of gas migration streamlines.The gas flow rate is characterized by streamline color. The tortuosity of pores and fissures is characterized by streamline size. The size of the connected channels between pores and fissures is characterized by streamline density.

The conclusions drawn from Figs. 15 and 16; Table 4 are as follows: The streamlines in the X, Y, and Z directions of REV are relatively scattered and there are many short and thin streamlines before HPAB. The streamline colors of the connecting channels between pores and fissures are mostly light blue and dark blue. The streamline colors at the minimum diameter of the connected channels and the intersection nodes of multiple channels are yellow and red. This indicates that Before HPAB, the connecting channels between the original pores and fissures in the coal were small in diameter and had a greater degree of tortuosity. As a result, gas tends to preferentially diffuse to the pores and fissures in coal with larger communication radius and smaller tortuosity. When gas migrates and diffuses to the smaller radius of connected channels and the intersection nodes of multiple channels, the gas migration rate increases. The maximum velocity of gas migration often occurs at the minimum radius of the connected channel. In REV, the maximum flow rate and velocity of gas migration in the X, Y, and Z directions are 7.784×10^{12} μm^3/s and 3.144×10^9 μm/s, respectively.

After HPAB, the number of sparse, short, and thin streamlines distributed in the X, Y, and Z directions in the REV decreased significantly. On the contrary, the dense, long, and thick streamlines distributed in the X, Y, and Z directions in the REV increased significantly. The maximum flow rate and maximum velocity of gas migration were greatly improved, with maximum flow rate and maximum velocity of 154.447×10^{12} μm^3/s and 16.465×10^9 μm/s, respectively. Compared with before HPAB, the maximum flow rate and maximum velocity have increased by 112.90 times and 5.24 times, respectively.

Conclusion

In this paper, Based on HPAB tests, the macroscopic fracture characteristics of coal under HAB were analyzed. A 3D visualization model of coal was established and visualized seepage simulation was carried out at the microscale before and after HPAB using industrial CT and Avizo software. The influence of pore fracture micro-pore structure on gas migration and permeability before and after HPAB is analyzed. the following conclusions are drawn:

(1) There are four main cracks on the coal surface that approximately run along the direction of principal stress under HPAB and confining pressure.The direction of crack development and propagation in coal under HPAB is influenced by natural defects such as joints and bedding. The complex 3D network structure

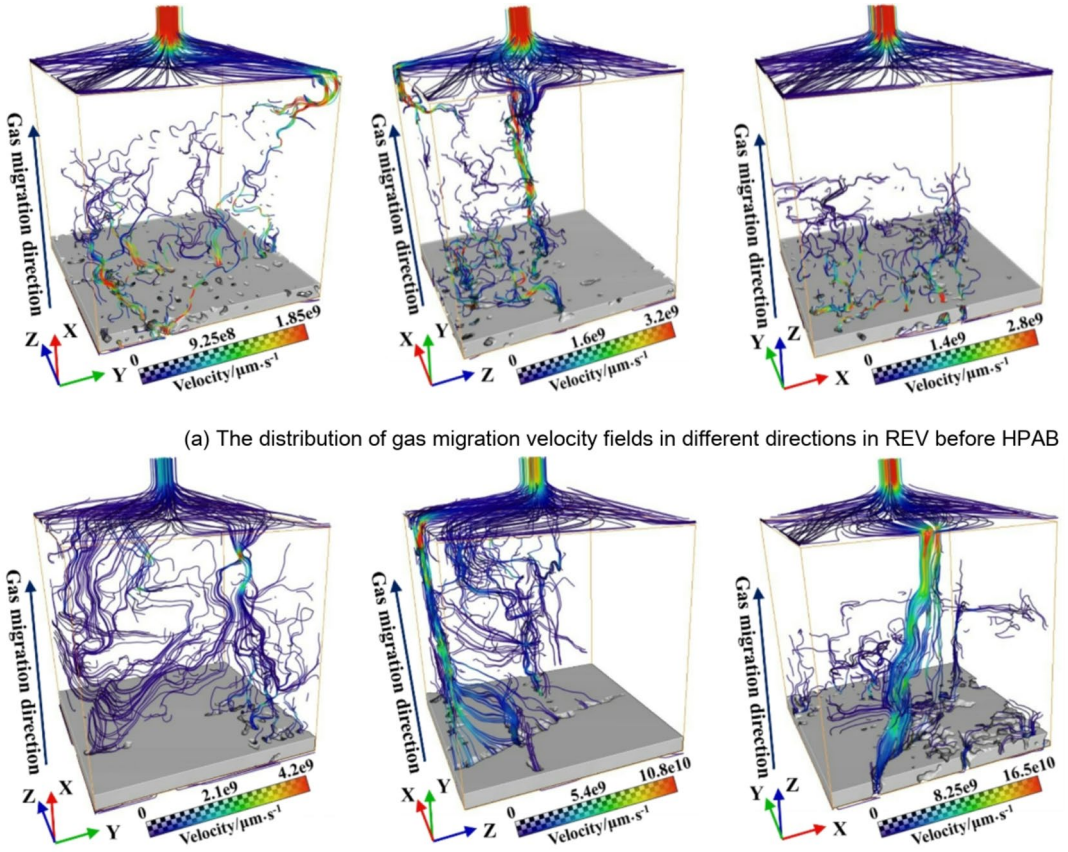

Fig. 15. The distribution of gas migration velocity fields in different directions in REV before and after HPAB.

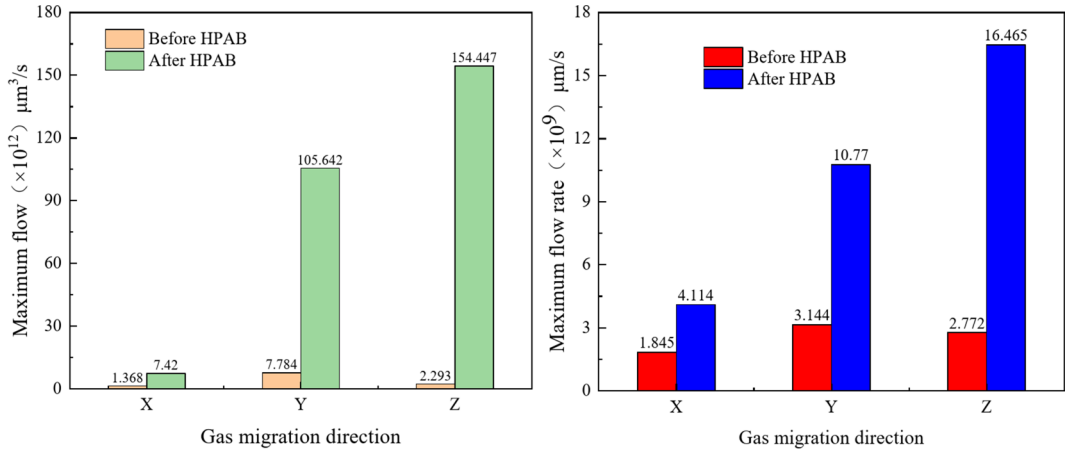

(a) The relationship between gas migration direction and maximum flow in REV before and after HPAB

(b) The relationship between gas migration direction and maximum flow rate in REV before and after HPAB

Fig. 16. The relationship between gas migration direction and maximum flow, maximum flow rate in REV before and after HPAB.

formed by the development and expansion of original micro-pores, fissures, and newly formed fractures has increased the porosity of coal under HPAB.

(2) The gas migration and diffusion pressure, velocity, and maximum flow rate of gas in the three-dimensional topological space of pores and fissures in the RVE of coal exhibit significant differences in X, Y, and Z three different directions. The size (radius and length) of pores and fissure connectivity in coal and the tortuosity of connected channels have a significant impact on the migration and expansion of gas.
(3) Before HPAB, The REV has a high degree of curvature in the connectivity channel. The gas migration pressure shows a decreasing trend during the migration process along the pore fissure connected channel.The pressure distribution range of gas migration in REV is relatively dispersed. Compared with before HPAB, After HPAB, the degree of curvature in REV is significantly reduced, with a decrease of up to 26.72%. The pressure of gas migration shows a steady-state decreasing trend, with gas migration pressure mostly concentrated in the range of 1.0 ~ 1.05 MPa. The maximum flow rate and maximum velocity have increased by 112.90 times and 5.24 times, respectively.

Data availability

All data generated or analysed during this study are included in this published article.

Received: 6 April 2025; Accepted: 8 August 2025
Published online: 14 August 2025

References

1. Xie, H. Research review of the state key research development program of china:deep rock mechanics and mining theory. *J. China Coal Soc.* **44** (5), 1283–1305. https://doi.org/10.13225/j.cnki.jccs.2019.6038 (2019).
2. Yuan, L. Research progress of mining response and disaster prevention and control in deep coal mines. *J. China Coal Soc.* **46** (3), 716–725. https://doi.org/10.13225/j.cnki.jccs.YT21.0158 (2021).
3. Wang, E., Zhang, G., Zhang, C. & Li, Z. Research progress and prospect on theory and technology for coal and gas outburst control and protection in China. *J. China Coal Soc.* **47** (01), 297–322. https://doi.org/10.13225/j.cnki.jccs.yg21.1846 (2022).
4. Yan, S. et al. Experimental study on dynamic response and damage evolution of coal under shocks by multiple high-pressure air blasting. *Geofluids* **2022** (2033679). https://doi.org/10.1155/2022/2033679 (2022).
5. Lv, J. et al. Technology of pressure relief and permeability enhancement with high pressure air blasting under high geo-stress. *J. China Coal Soc.* **44** (04), 1115–1128. https://doi.org/10.13225/j.cnki.jccs.2018.1053 (2019).
6. Zhang, S. et al. Development situation and trend of stimulation and reforming technology of coalbed methane. *Acta Petrolei Sinica.* **42** (01), 105–118. https://doi.org/10.7623/syxb202101010 (2021).
7. Wu, J., Liu, L., Zhao, G. & Chu, X. Research and exploration of high energy gas fracturing stimulation integrated technology in Chinese shale gas reservoir. *Adv. Mater. Res.* **524**, 1532–1536. https://doi.org/10.4028/www.scientific.net/AMR.524-527.1532 (2012).
8. Wu, F. et al. Numerical simulation and parametric analysis for designing high energy gas fracturing. *J. Nat. Gas Sci. Eng.* **53**, 218–236. https://doi.org/10.1016/j.jngse.2018.02.011 (2018).
9. Wang, L. et al. CO_2 injection-induced fracturing in naturally fractured shale rocks. *Energy* **139**, 1094–1110. https://doi.org/10.1016/j.energy.2017.08.031 (2017).
10. Gao, J. et al. Experimental study on High-pressure air blasting fracture for coal and rock mass. *Adv. Civ. Eng.* **2019**, 1–10 (2019). https://doi.org/10.1155/2019/9613563
11. Bai, Y., Sun, L. & Wei, C. A coupled gas flow-mechanical damage model and its numerical simulations on high energy gas fracturing. *Geofluids* **2020**, 1–14. https://doi.org/10.1155/2020/3070371 (2020).
12. Zhang, Y., Deng, J., Deng, H. & Ke, B. Peridynamics simulation of rock fracturing under liquid carbon dioxide blasting. *Int. J. Damage Mech.* **28** (7), 1038–1052 (2018). DOI:10.1177/1056789518807532.
13. Pan, H. et al. Study on crack propagation of the CO_2 presplitting blasting empty hole effect in coal seam. *Energy Sci. Eng.* **8** (11), 3898–3908. https://doi.org/10.1002/ese3.785 (2020).
14. Yang, X. et al. Study on the stress field and crack propagation of coal mass induced by High-pressure air blasting. *Minerals* **12** (3), 300. https://doi.org/10.3390/MIN12030300 (2022).
15. Chu, H. et al. Mechanism of nozzle position affecting coalbed methane mining in high-pressure air blasting. *Sustainability* **15**(14), 11171. 10.3390/su151411171 (2023).
16. Zhang, D. et al. Research and application on technology of increased permeability by liquid CO_2 phase change directional jet fracturing in low-permeability coal seam. *J. China Coal Soc.* **43**(07), 1938–1950. https://doi.org/10.13225/j.cnki.jccs.2018.0281 (2018).
17. Zhang, D. et al. Mechanism of breaking and fracture expansion of liquid CO_2 phase change jet fracturing in low-permeability coal seam. *J. China Coal Soc.* **43** (11), 3154–3168. https://doi.org/10.13225/j.cnki.jccs.2018.0946 (2018).
18. Yang, R. et al. Pore-scale analysis of coal structure and mechanical properties evolutionthrough liquid nitrogen thermal shock. *Nat. Gas. Ind.* **41** (07), 82–92. https://doi.org/10.3787/j.issn.1000-0976.2021.07.009 (2021).
19. Qin, L. et al. Changes in the pore structure of lignite after repeated cycles of liquid nitrogen freezing as determined by nitrogen adsorption and mercury intrusion. *Fuel* **267**, 117214. https://doi.org/10.1016/j.fuel.2020.117214 (2020).
20. Qin, L. et al. Evolution of the pore structure in coal subjected to freeze – thaw using liquid nitrogen to enhance coalbed methane extraction. *J. Petrol. Sci. Eng.* **175**, 129–139. https://doi.org/10.1016/j.petrol.2018.12.037 (2019).
21. Chu, Y. & Zhang, D. Study on the pore evolution law of anthracite coal under liquid nitrogen freeze-thaw cycles based on infrared thermal imaging and nuclear magnetic resonance. *Energy Sci. Eng.* **7** (6), 3344–3354. https://doi.org/10.1002/ese3.505 (2019).
22. Sun, Y. et al. Changes of coal molecular and pore structure under ultrasonic Stimulation. *Energy Fuels.* **35** (12), 9847–9859. https://doi.org/10.1021/acs.energyfuels.1c00621 (2021).
23. Lin, B. et al. Experimental study of the effect of NaCl solution on the pore structure of coal body with high-voltage electrical pulse treatments. *J. China Coal Soc.* **43** (05), 1328–1334. https://doi.org/10.13225/j.cnki.jccs.2017.1290 (2018).
24. Zhang, H. et al. Influence of local frequent dynamic disturbance on Micro-structure evolution of coal-rock and localization effect. *Nat. Resour. Res.* **29** (6), 3917–3942. https://doi.org/10.1007/s11053-020-09683-7 (2020).
25. Yan, S., Yang, X., Chu, H. & Wang, C. Experimental study on the dynamic response and pore structure evolution of coal under High-pressure air blasting. *ACS Omega.* **7** (28), 24475–24484. https://doi.org/10.1021/acsomega.2c02086 (2022).
26. Liao, Z. et al. Micro-structural damage to coal induced by liquid CO2 phase change fracturing. *Nat. Resour. Res.* **30** (2), 1613–1627. https://doi.org/10.1007/s11053-020-09782-5 (2021).

27. Wang, Y., Liang, W. & Yue, J. Research on the fractal characteristics of the micro/nano-mesoscopic pore structure of high-rank coal under impact loads. *Energy Sources Part A Recov. Utiliz. Environ. Effects* 1–18. (2020). https://doi.org/10.1080/15567036.2020.1809569
28. Li, M., Liang, W. & Yue, G. Fractal and pore structure analysis of structural anisotropic coal under different impact loads. *Environ. Earth Sci.* **79**, 1–16. https://doi.org/10.1007/s12665-020-09071-7 (2020).
29. Li, H. et al. Quantitative analysis of pore complexity in lacustrine Organic-Rich shale and comparison to marine shale: insights from experimental tests and fractal theory. *Energy Fuels*. **38** (17), 16171–16188. https://doi.org/10.1021/acs.energyfuels.4c03095 (2024).
30. Li, J. et al. Lithological controls on pore structure and their implications for deep shale gas reservoir quality in the longmaxi formation, Luzhou area, Southern Sichuan basin, China. *Energy Fuels*. **39** (3), 1541–1558. https://doi.org/10.1021/acs.energyfuels.4c05247 (2024).
31. Li, J. et al. Shale pore characteristics and their impact on the gas-bearing properties of the longmaxi formation in the Luzhou area. *Sci. Rep.* **14** (01), 16896. https://doi.org/10.1038/s41598-024-66759-7 (2024).
32. Xia, B. et al. Evaluation of liquid CO_2 phase change fracturing effect on coal using fractal theory. *Fuel* **287**, 119569. https://doi.org/10.1016/j.fuel.2020.119569 (2021).
33. Bai, X. et al. An enhanced coalbed methane recovery technique based on CO_2 phase transition jet coal-breaking behavior. *Fuel* **265**, 116912. https://doi.org/10.1016/j.fuel.2019.116912 (2020).
34. Yan, S. et al. Experimental study on crack propagation and vibration characteristics of coal under High-pressure air blasting. *Blasting* **42** (01), 142–150. https://doi.org/10.3963/j.issn.1001-487X.2025.01.017 (2025).
35. Hamed, A. et al. Pore-scale analysis of coal cleat network evolution through liquid nitrogen treatment: A Micro-Computed tomography investigation. *Int. J. Coal Geol.* **219**, 103370. https://doi.org/10.1016/j.coal.2019.103370 (2020).
36. Zhang, D. et al. An anisotropic pore-network model to estimate the shale gas permeability[J]. *Sci. Rep.* **11** (1), 7902. https://doi.org/10.1038/s41598-021-86829-4 (2021).

Acknowledgements

This study was supported by the National Key Research and Development Program of China (2023YFC2907202) and the National Natural Science Foundation of China (No.51874123) and the Key Science and Technology Research Projects of Henan Province (No.252102320172) and the Natural Science Foundation of Henan Province (242300421255).

Author contributions

For conceptualization, X.Y., S.Y., and H.C.; methodology, S.Y.; formal analysis, S.Y.; investigation, B.S.and C.W.; writing original draft preparation, S.Y.; writing-review and editing, F.G., X.Y. and H.C.; visualization, F.G. and S.Y. All authors have read andagreed to the published version of the manuscript.

Declarations

Competing interests

The authors declare no competing interests.

Additional information

Correspondence and requests for materials should be addressed to S.Y. or F.G.

Reprints and permissions information is available at www.nature.com/reprints.

Publisher's note Springer Nature remains neutral with regard to jurisdictional claims in published maps and institutional affiliations.